



Binding modes of cabazitaxel with the different human β -tubulin isotypes: DFT and MD studies

Lijuan Zhu¹ · Chao Zhang¹ · Xudong Lü¹ · Ce Song^{2,3} · Cuihong Wang⁴ · Meiling Zhang¹ · Yaoming Xie⁵ · Henry F. Schaefer III⁵

Received: 12 January 2020 / Accepted: 28 April 2020 / Published online: 30 May 2020
© Springer-Verlag GmbH Germany, part of Springer Nature 2020

Abstract

Taxanes (paclitaxel, docetaxel, cabazitaxel) are anticancer drugs as microtubule inhibitors. Following our previous studies on paclitaxel and docetaxel, in this work, we examine cabazitaxel and compare these three taxenes. The binding interaction of three taxenes with various β -tubulin isotypes is studied by homology modeling, molecular docking, and molecular dynamics simulations. The results show that the effects of docetaxel on β I-tubulin (-29.5 kcal/mol) and of paclitaxel on β Ia-tubulin (-25.5 kcal/mol) are much stronger than their effects on β III-tubulin (-17.8 kcal/mol and -8.6 kcal/mol, respectively). However, the effect of cabazitaxel on β III-tubulin (-23.0 kcal/mol) is comparable with that on β I-tubulin (-24.0 kcal/mol) and β Ia-tubulin (-25.9 kcal/mol), consistent with the fact that overexpression of β III-tubulin increases the drug resistance to paclitaxel and docetaxel, but has little influence for cabazitaxel. This theoretical research supports the use of cabazitaxel for patients who are resistant to the action of paclitaxel and docetaxel.

Keywords Cabazitaxel · β -Tubulin isotypes · Taxenes · DFT methods · MD simulations · Drug resistance

Introduction

According to the 2018 National Cancer Report, the highest morbidity among men is prostate cancer, and that among women is breast cancer considering all malignancies in the

US, and they rank second only to heart disease [1]. The latest cancer data show that morbidity and mortality of various malignant tumors are rising, and tumors are likely to remain one of the major causes of death [2–5].

Microtubules (MTs), made up of polymerized α - and β -tubulin dimers, play a very important role in many cellular processes, including the cancer cellular process [6]. MTs are involved in the development and maintenance of cell shape, cell motility, intracellular transport, cell division, and mitosis [7, 8]. Microtubule inhibitors (MTIs) such as taxanes, epothilones, vinca alkaloids, and colchicines effectively block cancer cell division by changing the microtubule dynamics (either assembly or disassembly) required for proper mitosis. The action sites of the classical MTIs are shown in Fig. 1 [8–14].

Taxane anticancer drugs, a class of diterpenes, are common drugs of MTIs [17]. There are mainly three analogs used in clinical applications, namely, paclitaxel (PTX), docetaxel (DTX), and cabazitaxel (CTX). The binding sites of taxanes are on β -tubulin as shown in Fig. 1 [18–24]. PTX is the first generation of taxanes. In 1992, it was approved for the treatment of advanced non-small cell lung cancer, breast cancer, and ovarian cancer by the Food and Drug Administration (FDA) [17, 25], and recently, it has also been used to treat

Electronic supplementary material The online version of this article (<https://doi.org/10.1007/s00894-020-04400-w>) contains supplementary material, which is available to authorized users.

✉ Meiling Zhang
mlzhang@tmu.edu.cn; zhm@mail.ustc.edu.cn

¹ School of Biomedical Engineering and Technology, Tianjin Medical University, 22 Qixiangtai Road, Tianjin 300070, China

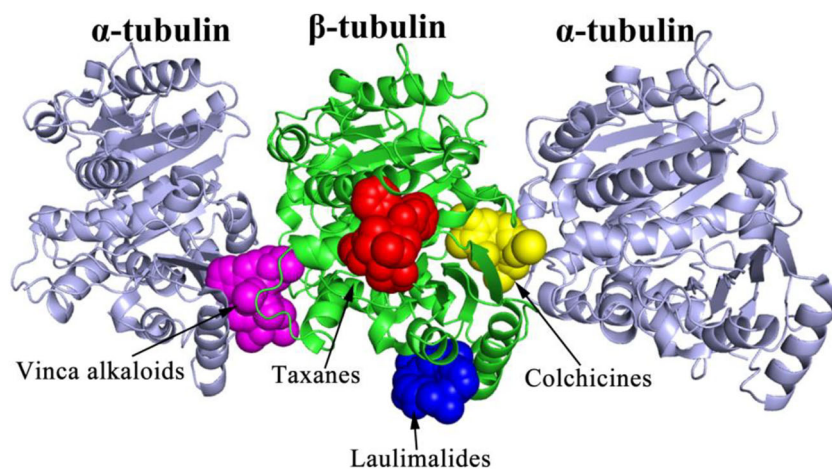
² Hefei National Laboratory of Physical Sciences at the Microscale, University of Science and Technology of China, Hefei 230026, Anhui, China

³ Department of Theoretical Chemistry and Biology, School of Biotechnology, Royal Institute of Technology, SE-10691 Stockholm, Sweden

⁴ School of Science, Tianjin Chengjian University, 26 Jinjing road, Tianjin 300384, China

⁵ Center for Computational Quantum Chemistry, University of Georgia, Athens, GA 30602, USA

Fig. 1 Structural overview of microtubule-inhibitor action sites on tubulin dimers. The action sites of taxanes, epothilones, and vinca alkaloids are on β -tubulin, and the sites of colchicines are at the $\alpha\beta$ -tubulin dimer interface [15, 16]



Kaposi sarcoma, cervical cancer, and pancreatic cancer [26–28]. Subsequently, researchers synthesized a second-generation compound DTX, with better water solubility and lesser adverse reactions, by modifying the PTX side chains [29]. In 1996, DTX was approved by the FDA to treat early or advanced breast cancer [30], and it is the main chemotherapy drug used in current clinical treatments for the metastatic castrate-resistant prostate cancer (mCRPC) [31]. DTX is found to be effective for most patients, but it is easy to develop tolerance [32]. To solve the drug resistance problem, researchers synthesized a third-generation compound CTX, which was approved by the FDA in 2010 to treat the metastatic prostate cancer [33, 34], and CTX is used as a second-line treatment for mCRPC patients [35, 36].

There are many tubulin isotypes (such as β I-tubulin, β II-tubulin, and β III-tubulin) in the human body, and the identified β -tubulin isotypes are expressed differently in different cell types [37–40]. In particular, the expression of β III-tubulin isotype is often associated with drug-resistant and aggressive cancers [41–44]. It was reported that the amount of β III-tubulin was relatively low at the early time of treatment, and PTX and DTX were effective [45–47]. However, after the treatment, the amount of β III-tubulin increases, and then, the effects of PTX and DTX begin to wear off [32, 48]. Smiyun et al. reported that CTX was effective for those patients who were resistant to DTX [49].

Since there are still many limitations in clinical tests [50–55], the detailed action mechanism of different isotypes with taxanes remains unclear. In the present study, we will theoretically explore drug-binding modes and drug resistance of taxanes interacting with different tubulin isotypes. Our previous studies [24, 56] have predicted the lowest-lying conformations of the PTX and DTX with Density Functional Theory (DFT) methods. In the present paper, we will optimize the structure of CTX with the same methods. We will further build three-dimensional models of the human tubulin isotypes by homology modeling and then examine the tubulin isotypes

with higher binding affinities to taxanes using the molecular docking method. Since the drug binding on the protein and the molecular recognition is a dynamic process [57], we will also investigate the detailed active sites and binding affinities of these processes using molecular dynamics (MD) simulations.

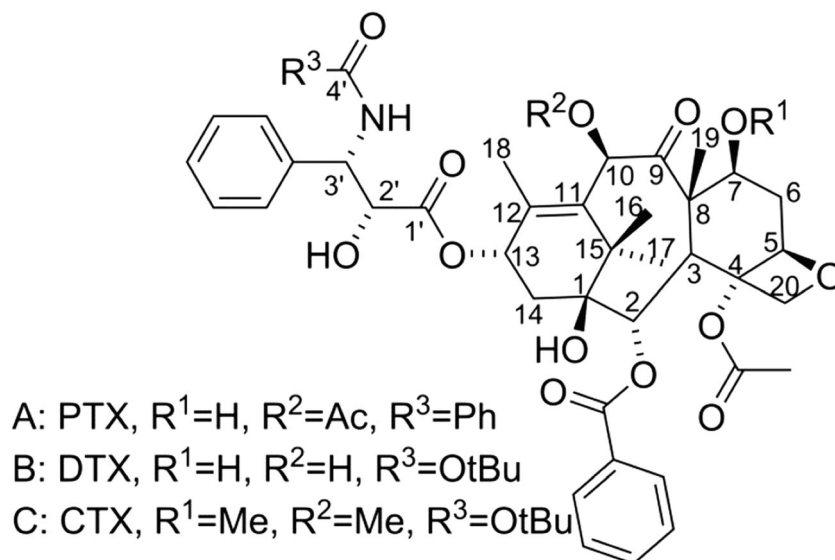
Computational methods

Optimization molecular structure of CTX

The taxanes studied in the present paper include PTX, DTX and CTX (Fig. 2). The optimized geometries of PTX and DTX have been reported previously [24, 56], and the molecular geometry of CTX was optimized here. The initial structure of CTX was generated by modifying the lowest-lying DTX structure. The Gaussian16 software [58] was used to search the possible global minima. To avoid missing any promising structures, the full conformational space of gaseous CTX was explored through a systematic variation of rotational degrees of freedom around seven bonds in the C13 side chain, as shown in Fig. 3. The dihedral angle for each bond can be varied from 0 to 360° with the increment of 60° for six asymmetric rotations or the increment 120° for one symmetrical rotation. Thus, 139,968 initial conformations were generated.

We initially used the semi-empirical PM7 method, and then, the HF/3-21G* method to remove distracting conformations such as those with imaginary vibrational frequencies. Then, we used the B3LYP/6-311G* method to obtain gaseous conformations. The vibrational frequency analysis was carried out at the same level of theory. More accurate relative energies were obtained from single-point energies at the M06-L/6-311G(2df,p) level in both the gaseous phase and water solution (with the polarizable continuum model). Finally, the excited states of the lowest-lying CTX conformation were studied with the TD DFT method, namely, the CAM-B3LYP/6-311+G(2df,p).

Fig. 2 Structures of PTX (A), DTX (B), and CTX (C). The parental ring structures of three taxanes are the same, but the C7, C10, and C13 side chains are different



Homology modeling

Homology modeling is a method to construct an atomic-resolution model of the “target” protein from its amino acid sequence and an experimentally known three-dimensional structure of a related homologous “template” protein [59]. It can produce high-quality structural models when the target and template are closely related.

In the present study, we adopted homology modeling to build the three-dimensional models for different isotypes of the human $\alpha\beta$ -tubulin. The “template” $\alpha\beta$ -tubulin, including GTP (Guanosine triphosphate), GDP (Guanosine iphosphate), PTX, and Mg^{2+} bound to it, was taken from the high-

resolution cryo-electron microscopy structure of microtubule (PDB ID: 5SYF.pdb, resolved at 3.5 Å, shown in Fig. S1 in Supplementary Material) [22]. The amino acid sequences of the human tubulin were collected from the UniProt protein sequence database (www.uniprot.org) [60]. We used the online tool Clustal Omega (www.ebi.ac.uk/Tools/msa/clustalo) for multiple sequence alignment analysis [61] and then used SWISS-MODEL (www.swissmodel.expasy.org) for single template modeling [62–66].

Molecular docking

Molecular docking is a method of molecular simulation to predict the preferential orientation of one molecule binding with another when they form a stable complex. It is one of the most common methods to predict the binding conformation of a ligand with a suitable protein target [67].

In the present study, molecular docking was performed using the AutoDock4.2 software [68]. At first, a larger box with the $126 \times 126 \times 126$ grid and the grid spacing of 1.0 Å was adopted for the global docking of the $\alpha\beta$ -tubulin dimer with CTX to find the binding sites of CTX on tubulin dimer. And then, the different human tubulin isotypes with the lowest-lying PTX, DTX and CTX conformations were used for the local docking on the binding sites we found. The local docking was performed with a smaller box with a finer grid of $60 \times 60 \times 60$ and the grid spacing of 0.375 Å. Using the Lamarckian Genetic Algorithm (LGA) for generating binding poses, we set the maximum number of energy evaluations to be 25 million. A total of 100 runs were performed, and for every independent run, a maximum number of 27,000 generations were investigated on a single population of 150 individuals.

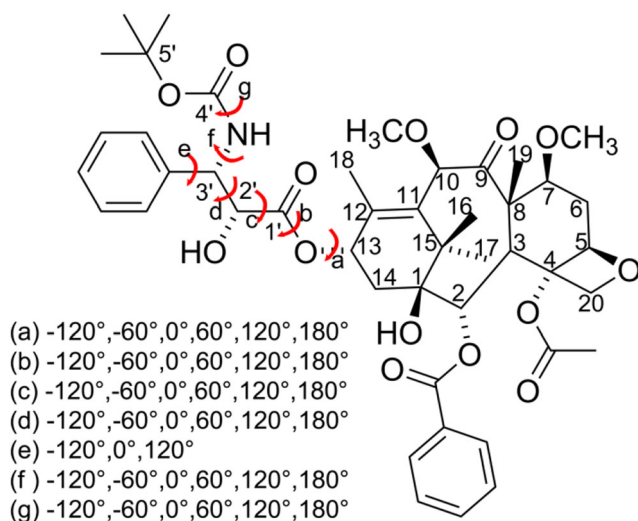


Fig. 3 The degrees of freedom for CTX. For the C13 side chain of CTX, a total of seven rotatable bonds (a–g) were selected. We chose 60° as the incremental rotation for each rotational torsion angle except for (e); the increment of which is 120° due to the local symmetry

Molecular dynamics simulations

The MD simulations were performed for the complexes with high-binding energy between the three taxanes and different tubulin isotypes with the AMBER99SB-LIDN force field from the GROMACS5.0 software [69]. The general Amber force field (GAFF) for PTX, DTX, and CTX was obtained from the antechamber module of AmberTools12 [70]. The systems were immersed in a dodecahedral box of SPC/E waters during simulation [71], where there was a buffer of 1.0 nm between the protein atoms and the edge of the water box. We added Na⁺ or Cl⁻ ions to make them neutral. The steepest descent method was used for energy minimization. Then NVT ensemble, whose positions were restrained by the LINC algorithm [72], and NPT ensemble, whose temperature was increased from 0 to 300 K under the standard atmospheric pressure, were performed for 1 ns, respectively, and finally, the production simulation was performed for 100 ns with a time step of 2 fs. According to literatures [32, 41, 47, 73–75], the drug effect became weak if β III-tubulin overexpressed in cancer cells. In order to rationalize this phenomenon, the same MD simulations were also performed for the complexes of β III-tubulin and three taxanes. The details are presented in Table S1 (Supplementary Material).

With the MD results, we could further assess the free binding energies between β -tubulin and taxanes.

$$\Delta G_{\text{bind}} = G_{\text{complex}} - G_{\text{free-protein}} - G_{\text{free-ligand}} \quad (1)$$

where G_{complex} , $G_{\text{free-protein}}$, and $G_{\text{free-ligand}}$ are free energies for the complex, protein, and ligand, respectively. The MM-PBSA (Molecular Mechanics Poisson-Boltzmann Surface Area) method [76, 77] implemented in the *g_mmpbsa* program [78] is adopted, and the parameters used here are presented in Table S1 (Supplementary Material). The method of total free energy calculation is referred to [76, 77], which is the summation of gas phase energy and the solvation energy. Note that the solvation free energy can be decomposed into polar and non-polar contributions. For the polar solvation energy, the implicit solvent model ($\epsilon = 2.0$) was used. (The other values of dielectric constant were also tried, but the conclusions are essentially the same.) For the non-polar solvation energy, the solvent-accessible surface area (SASA) model was used.

Results and discussion

Optimization molecular structure of CTX

After the PM7 and HF screening, 100 conformations were left out of the initial 139,968 conformations generated by the internal rotations as shown in Fig. 3. Finally, the 20 most stable

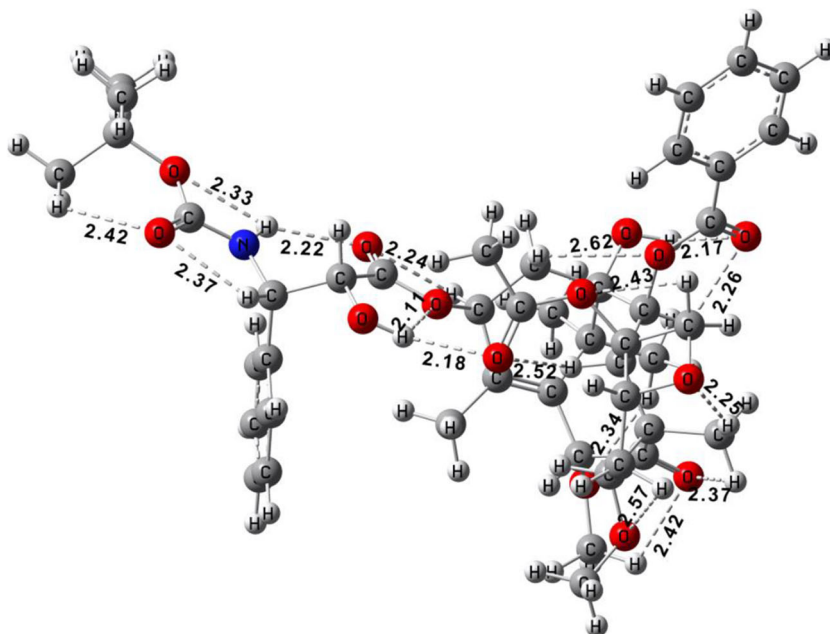
CTX conformations in the gas phase were obtained at the B3LYP/6-311G* level. The single-point energies were evaluated at the M06-L/6-311G(2df,p) level in both the gas phase and aqueous solution. Table 1 shows the theoretical relative energies, the zero point vibrational energies (ZPVE), the rotational constants, and the dipole moments for these 20 conformations. The lowest-lying CTX conformation (conformation 1, shown in Fig. 4) was found to be the global minimum in both gas phase and solution, and conformation 1 was used for the subsequent studies.

The hydrogen bonds in the lowest-lying CTX conformation (conformation 1), taking a cutoff distance of 2.8 Å between the H-bonding donor and acceptor, are shown in Fig. 4. It is found that the main hydrogen bond acceptors in CTX are O and N atoms, and the main donors are –NH and –OH groups. The weak hydrogen bonds with the –CH groups as H-bonding donors are also found. As shown in Fig. 4, there are 17 hydrogen bonds in conformation 1. To discuss these hydrogen bonds, we compared them in conformation 1 with those in other conformations (conformations 2 and 3, Fig. S2 in Supplementary Material). There are two differences among these three conformations. At first, the –NH donor in conformation 1 forms two hydrogen bonds with the O atom of C4'-O-C5' and C1'=O (with distances of 2.33 Å and 2.22 Å), while the –NH group in conformations 2 and 3 only interacts with the O atom of C4'-O-C5' (with distances of 2.32 Å and 2.33 Å, respectively). Secondly, the –OH donor on C2' forms two conventional hydrogen bonds with the O atom of C13-O-C1' and C=O (linked to C4) in conformation 1 (with the distances of 2.11 Å and 2.18 Å) and in conformation 3 (with the distances of 2.19 Å and 2.03 Å), while the –OH on C2' in conformation 2 only interacts with the O atom of C=O (linked to C4) by 2.06 Å. It may be further inferred that, with significant structural flexibility in larger biomolecules, the coexistence of dihydrogen bonds, as well as many red-shifting hydrogen bonds, should be a common phenomenon and have important effects on the conformational energetics and other properties.

Our theoretical IR spectra for the lowest three conformations predicted with the B3LYP/6-311G* method (scaled by a factor of 0.96) [79] are shown in Fig. 5. The values for harmonic vibrational frequencies with strong infrared intensities for several representative CTX conformations are also reported in Table 2. Figure 5a shows that there are a number of strong absorption peaks in the range of 1000 to 1300 cm⁻¹, which are corresponding to the normal modes assigned as the C–O–C stretching, benzene ring deformation, and methyl group wagging. Our theoretical results are basically in agreement with the experimental IR observation of 1270, 1246 cm⁻¹ assigned for the C–O–C (ester) stretching modes and of 1170, and 1026 cm⁻¹ assigned for the C–O–C (ether) stretching modes [80]. The vibrational frequencies ranged from 2850 to 3100 cm⁻¹ (Fig. 5b) are corresponding to the

Table 1 Relative energies, relative zero-point vibrational energies, rotational constants, and dipole moments of the 20 most stable CTX conformations

Conformation	Relative energy (kcal/mol)				Rotational constants ^c (GHZ)			Dipole moment ^c (Debye)
	B3LYP ^a	M06L ^b	M06Ls ^c	ZPVE ^d	A	B	C	
1	0.00	0.00	0.00	0.00	0.058	0.028	0.023	2.31
2	0.48	0.57	2.01	-0.46	0.053	0.033	0.030	5.20
3	2.72	1.91	3.29	-0.25	0.054	0.033	0.026	8.61
4	2.20	2.62	1.19	-0.10	0.059	0.028	0.023	3.23
5	3.23	2.90	4.94	0.05	0.054	0.032	0.030	4.55
6	3.17	3.09	3.76	0.03	0.059	0.028	0.023	2.68
7	4.68	3.21	5.12	-0.07	0.061	0.035	0.029	4.24
8	4.05	3.66	3.12	-0.49	0.062	0.028	0.024	4.71
9	6.62	3.66	3.12	-0.25	0.062	0.028	0.024	4.71
10	4.70	3.87	4.98	0.08	0.062	0.027	0.023	4.79
11	5.51	4.39	6.98	-0.11	0.054	0.032	0.026	7.42
12	2.08	4.65	1.33	0.33	0.060	0.028	0.024	5.01
13	4.88	4.70	7.54	0.13	0.055	0.035	0.029	5.34
14	4.37	5.01	4.18	0.13	0.057	0.029	0.028	5.77
15	6.98	5.41	5.76	-0.20	0.054	0.037	0.029	4.13
16	6.85	5.81	6.35	0.24	0.063	0.028	0.024	3.99
17	5.69	5.89	6.05	-0.64	0.056	0.031	0.028	5.49
18	4.72	6.23	6.60	-0.29	0.055	0.027	0.024	7.44
19	8.02	6.36	7.96	-0.03	0.057	0.032	0.028	4.95
20	7.68	6.42	5.23	-0.07	0.055	0.035	0.028	7.94

^a Geometry optimization at the B3LYP/6-311G* level^b Single-point energies at the M06-L/6-311G(2df,p)//B3LYP/6-311G* level^c Energies, rotational constants, and dipole moments at the M06-L/6-311G(2df,p)//B3LYP/6-311G* level in a solution using the polarizable continuum model^d The relative ZPVEs at the B3LYP/6-311G* level, scaled by a factor of 0.96 [79]**Fig. 4** The lowest-lying CTX conformation (conformation 1) in the gas phase at the B3LYP//6-311G* level. The important hydrogen bonds are represented by dotted lines

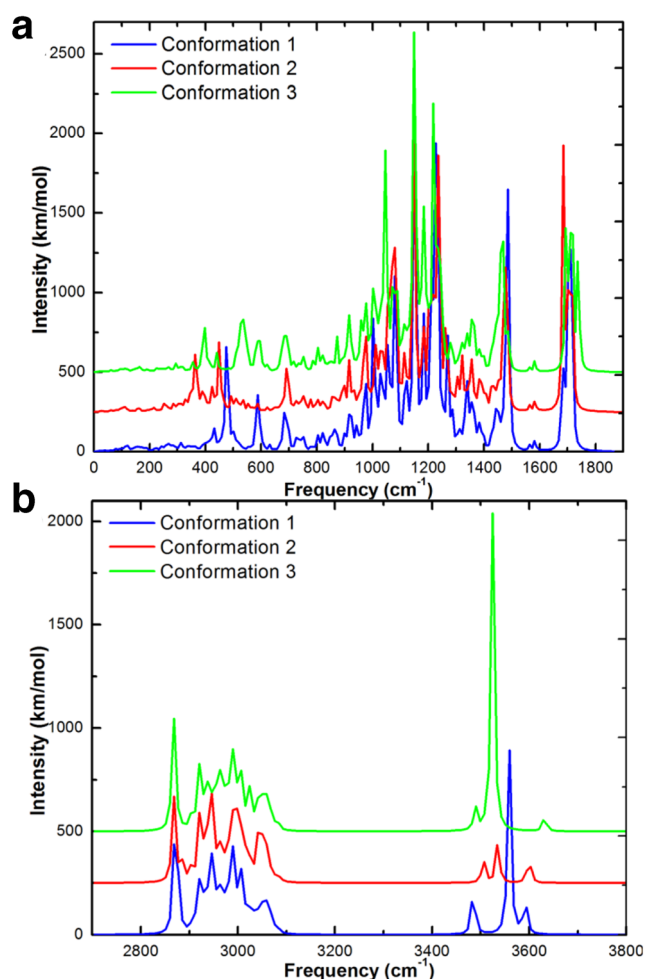


Fig. 5 Our predicted IR spectra of the three lowest-lying CTX conformations at the B3LYP/6-311G* level: **a** in the range of 0–1900 cm^{-1} and **b** in the range of 2700–3800 cm^{-1}

assignments of the C–H stretching in methyl, methylene, and methoxy groups, which agree with the experimental value at

2822 to 2980 cm^{-1} [80]. These C–H stretching modes in different conformations are almost identical, since the C–H bonds are usually transferable among molecules.

However, the frequencies related to the O–H stretching modes have an obvious shift among the different conformations, and this reflects the big change of bond strength when H-bond formation occurs. As shown in Table 2, the stretching frequency of O–H on C2' in conformation 1 (3559 cm^{-1}) is blue-shifted by about 34 cm^{-1} relative to that in conformation 3 (3525 cm^{-1}), indicating a stronger hydrogen bond between the O–H and C=O (linked to C4) groups in conformation 3. The O–H stretching frequency on C1 in conformation 1 (3591 cm^{-1}) is red-shifted by about 45 cm^{-1} relative to that in conformation 3 (3632 cm^{-1}) and conformation 13 (3637 cm^{-1}), due to the hydrogen bond between the O–H and the C=O (in PhCOO⁻) groups in conformation 1.

Table 2 shows that five strong IR frequencies of C=O stretching modes for conformation 1 are in the range of 1682–1718 cm^{-1} . For other conformations, the ranges of these five frequencies are almost the same, and these values are in agreement with the experimental assignment for CTX, which is a very strong peak at 1723 cm^{-1} [80]. When a C=O group is involved in a hydrogen bond, this C=O stretching frequency would be red-shifted. For example, the C=O frequency is red-shifted by 36 cm^{-1} for the C9 = O bond compared with that for the C=O bond linked on C2, because a stronger hydrogen bond is for the former.

The ultraviolet absorption of the molecule reflects the electronic transitions to the higher excited states. We explored the three lowest excited electronic states of the CTX (conformation 1) with the time-dependent (TD) method at the CAM-B3LYP/6-311+G(2df,p) level in methanol solution. Table 3 reports the excited energies, dipole transition oscillator strengths, excitations, and types of orbital transitions of the lowest-lying CTX. The orbitals involved in these excitations

Table 2 Harmonic vibrational frequencies (freq; cm^{-1}) scaled by a factor of 0.96 [79] and the IR intensities (int; km/mol) for the representative vibrational modes of some CTX conformations at the B3LYP/6-311G* level

Vibrational mode	Conformation 1		Conformation 2		Conformation 3		Conformation 13		Conformation 20	
	Freq	Int	Freq	Int	Freq	Int	Freq	Int	Freq	Int
N–H stretch	3485	79	3506	37	3489	33	3491	40	3499	53
O–H stretch on C1	3591	56	3599	43	3632	25	3637	20	3594	55
O–H stretch on C2'	3559	268	3535	62	3525	456	3527	85	3552	46
C–H sym stretch of Bz ring on C2	3063	29	3062	31	3064	29	3063	27	3065	23
C–H sym stretch of Bz ring on C3'	3056	36	3049	35	3052	36	3053	35	3052	39
C=O stretch on C2	1682	187	1683	201	1711	127	1705	26	1680	182
C=O stretch on C4	1700	245	1714	199	1693	234	1714	185	1713	393
C=O stretch on C4'	1707	305	1687	377	1706	192	1705	26	1706	192
C=O stretch on C1'	1713	179	1704	204	1739	250	1704	271	1714	56
C=O stretch on C9	1718	139	1718	139	1719	203	1674	293	1717	240

Table 3 Electronic excitation energies (ΔE), dipole transition oscillator strengths (f), excitation orbitals, and the type of orbital transition for the lowest three UV excitations of the lowest-lying CTX conformation at the TD CAM-B3LYP/6-311+G(2df,p) level

Excited state	ΔE (eV)	λ (nm)	f	Excitation	Coefficient	Type of orbital transition
S_0-S_1	4.27	291	0.0028	HOMO-12 \rightarrow LUMO+1	-0.137	$n \rightarrow \sigma^*$
				HOMO-11 \rightarrow LUMO+1	0.118	$n \rightarrow \sigma^*$
				HOMO-7 \rightarrow LUMO+1	0.100	$n \rightarrow \sigma^*$
				HOMO-3 \rightarrow LUMO+1	-0.406	$n \rightarrow \sigma^*$
				HOMO \rightarrow LUMO+1	0.397	$n \rightarrow \sigma^*$
S_0-S_2	5.10	243	0.0315	HOMO-7 \rightarrow LUMO	-0.105	$n \rightarrow \sigma^*$, $n \rightarrow \pi^*$
				HOMO-5 \rightarrow LUMO+3	-0.279	$n \rightarrow \pi^*$, $\pi \rightarrow \pi^*$
				HOMO-4 \rightarrow LUMO	0.618	$\pi \rightarrow \sigma^*$, $\pi \rightarrow \pi^*$
S_0-S_3	5.43	228	0.0929	HOMO-16 \rightarrow LUMO	0.413	$n \rightarrow \sigma^*$, $n \rightarrow \pi^*$
				HOMO-15 \rightarrow LUMO	-0.149	$n \rightarrow \sigma^*$, $n \rightarrow \pi^*$
				HOMO-13 \rightarrow LUMO	0.271	$n \rightarrow \sigma^*$, $n \rightarrow \pi^*$
				HOMO-12 \rightarrow LUMO	0.137	$n \rightarrow \sigma^*$, $n \rightarrow \pi^*$
				HOMO-11 \rightarrow LUMO	0.111	$n \rightarrow \sigma^*$, $n \rightarrow \pi^*$
				HOMO-5 \rightarrow LUMO	0.345	$n \rightarrow \sigma^*$, $n \rightarrow \pi^*$, $\pi \rightarrow \sigma^*$, $\pi \rightarrow \pi^*$

are displayed in Fig. S3 (Supplementary Material). Although some of these orbitals are delocalized on the phenyl rings as well as on the N and O atoms, we can approximately assign HOMO-4, HOMO-5 as π orbital on the benzene rings, while HOMO, HOMO-3, HOMO-4, HOMO-5, HOMO-7, HOMO-11, HOMO-12, HOMO-13, HOMO-15, HOMO-16 orbitals have components of the N and O lone pairs (symbol n in Table 3). The virtual orbitals LUMO and LUMO+3 are the π^* orbitals on the phenyl ring, and the orbitals LUMO, LUMO+1 have components of the σ^* orbital on the C and O atoms. The UV spectrum of the three excitations for CTX is predicted to be 228–291 nm (Table 3). The S_0-S_1 transition at 4.25 eV (291 nm) is an $n \rightarrow \sigma^*$ transition with weak oscillator strength (0.0028). The S_0-S_2 transition at 5.10 eV (243 nm) is a mixed $n\sigma^*/\pi\sigma^*/n\pi^*/\pi\pi^*$ transition, and the S_0-S_3 transition at 5.43 eV (228 nm) is also a mixed $n\sigma^*/\pi\sigma^*/n\pi^*/\pi\pi^*$ transition.

Sequence analysis and homology modeling

Nine human β -tubulin sequences were collected from the UniProt database [60], namely, β I-tubulin isotype (UniProt ID = Q9H4B7), β IIa-tubulin isotype (UniProt ID = Q13885), β IIb-tubulin isotype (UniProt ID = Q9BVA1), β III-tubulin isotype (UniProt ID = Q13509), β IVa-tubulin isotype (UniProt ID = P04350), β IVb-tubulin isotype (UniProt ID = P68371), β V-tubulin isotype (UniProt ID = P07437), β VI-tubulin isotype (UniProt ID = Q9BUF5), and β VIII-tubulin isotype (UniProt ID = Q3ZCM7), and they all were used as target proteins. With the template protein of $\alpha\beta$ -tubulin dimer (PDB ID = 5SYF.pdb [22] UniProt ID = P02554) taken from the cryo-electron microscopy structure, the results of multiple

alignments are shown in Table 4 and Table S2 (Supplementary Material). The identities between the target proteins and the template protein are very high, all larger than 90% except for β I-tubulin (78%) and β VIII-tubulin (88%). The identity of β II-tubulin to the template is even as high as 98.7%. It was suggested that high-accuracy comparative models are based on more than 50% sequence identity [81]. Therefore, these target proteins in our work are reliable for homology modeling to the construction of the 3D structure models.

The homology modeling for the nine $\alpha\beta$ -tubulin isotypes was done with the online tool SWISS-MODEL [62–66]. The results from the homology modeling were also assessed by the Verify-3D program [82, 83]. The good scores (> 94%, Table 4) of the assessment for the nine human β -tubulin isotypes further indicate that all these structures are reliable for the docking studies.

Molecular docking

The preliminary global docking results for the 20 lowest-lying CTX conformations with the $\alpha\beta$ -tubulin dimer are shown in Fig. 6 and Table S3 (Supplementary Material). Eighteen CTX conformations are located on β -tubulin (N1), one (conformation 18) located on $\alpha\beta$ -tubulin dimer interface (N2), and one (conformation 5) on α -tubulin (N3). As shown in Table S3, the binding energies of CTX conformations docked on β -tubulin (N1) are stronger than that on $\alpha\beta$ -tubulin dimer interface (N2) or on α -tubulin (N3). For example, the binding energy of conformation 1 docked on β -tubulin is -9.74 kcal/mol, while those on $\alpha\beta$ -tubulin dimer interface and on α -tubulin are -7.68 kcal/mol and -6.58 kcal/mol,

Table 4 Identity of the nine target human β -tubulin isotypes to the template tubulin dimer (5SYF.pdb), the number of amino acid sequences for the target β -tubulin isotypes, and the assessment for the homology modeling results by Verify-3D program [82, 83]

β -tubulin isotype	UniProt ID	Identity (%)	The number of β -tubulin amino acid sequence	Verify-3D assessment ^a (%)
β I-tubulin	TBB1	78.4	451	95.5
β IIa-tubulin	TBB2A	98.7	445	95.5
β IIb-tubulin	TBB2B	98.7	445	95.5
β III-tubulin	TBB3	92.6	450	94.8
β IVa-tubulin	TBB4A	96.2	444	95.1
β IVb-tubulin	TBB4B	97.5	445	95.5
β V-tubulin	TBB5	96.2	444	95.5
β VI-tubulin	TBB6	90.8	446	95.1
β VIII-tubulin	TBB8	88.3	444	96.9

^a The percentage of the residues with averaged 3D-1D score ≥ 0.2

respectively. Similar to the previous research on PTX and DTX [16, 19–24], the taxanes, including CTX, are found to act mainly on β -tubulin, so the further local docking is simply carried out between the taxanes and different isotypes of β -tubulin.

The local docking results of PTX, DTX and CTX with different β -tubulin isotypes, including the binding affinities and the residues related to the formation of hydrogen bonds, are shown in Table 5. The most common human β -tubulin isotypes (β I-tubulin and β II-tubulin) have significant binding affinities (Table 5). For example, the three strongest binding affinities for PTX are onto β I-tubulin, β IIa-tubulin, and β IIb-tubulin (–9.01, –9.84, and –9.98 kcal/mol, respectively), those for DTX are onto β I-tubulin, β IIa-tubulin, and β IIb-tubulin (–8.83, –8.60, and –8.85 kcal/mol, respectively), and those for CTX are onto β IIa-tubulin, β IIb-tubulin, and β III-tubulin (–8.69, –8.55, and –8.52 kcal/mol, respectively). Generally speaking, among these β -tubulin isotypes, β I-tubulin and β II-

tubulin have stronger binding affinities with the taxanes, indicating that they are the leading action of proteins with taxanes. Our docking results show that β III-tubulin isotype has weaker binding energy than β I-tubulin isotype with PTX and DTX, and this confirms the experimental studies that the overexpression of β III-tubulin may reduce the action of taxanes [32, 41, 47, 73–75].

Docking modeling provides the number of hydrogen bonds formed between the taxanes and tubulins (Table 5). For β IIa-tubulin, there are two hydrogen bonds docking with PTX and only one with DTX and CTX. The binding affinity of PTX (–9.84 kcal/mol) with β IIa-tubulin is accordingly stronger than those of DTX and CTX (–8.60 and –8.69 kcal/mol). Table 5 also shows that the main acting sites in all β -tubulin isotypes docking with the three taxanes are the amino acid residues His227, Pro272, Thr274, Arg276, Arg359, and Gly360. More detailed docking information is available in Table S4 (Supplementary Material), including the bond geometry parameters and the bond energies.

Fig. 6 The binding sites of the lowest-lying 20 CTX conformations on $\alpha\beta$ -tubulin dimer found by docking, where N1 is located on β -tubulin, N2 is located on $\alpha\beta$ -tubulin dimer interface, and N3 is located on α -tubulin

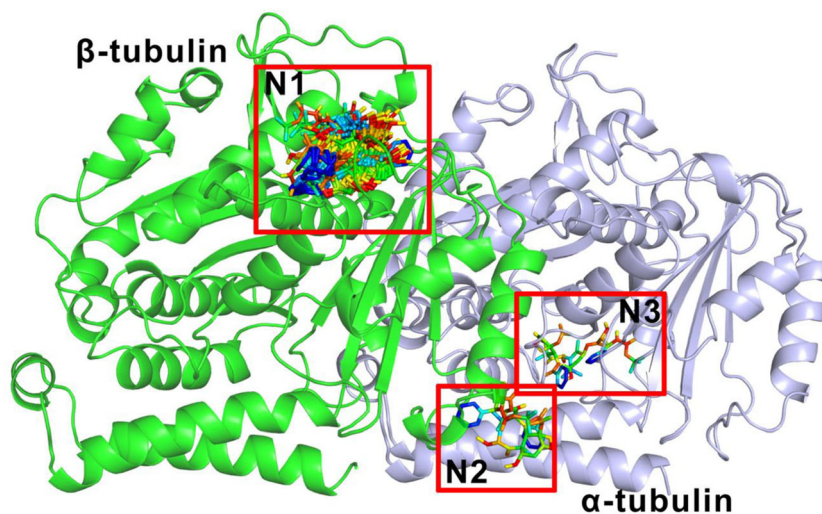


Table 5 Binding affinity from molecular docking and the residues about hydrogen bonds for PTX, DTX and CTX with β -tubulin isotypes

Taxane	β -tubulin	Binding affinity (kcal/mol)	Number of H-bonds	Residues about H-bonds
PTX	β I-tubulin	-9.01	2	Gln276, Gly360
	β IIa-tubulin	-9.84	2	Thr274
	β IIb-tubulin	-9.98	1	Thr274
	β III-tubulin	-8.91	2	Thr274, Arg359
	β IVa-tubulin	-8.86	3	His227, Thr274
	β IVb-tubulin	-8.92	3	His227, Thr274, Arg359
	β V-tubulin	-8.91	2	Thr274, Arg359
	β VI-tubulin	-8.82	2	Thr274, Arg359
DTX	β VIII-tubulin	-8.89	1	Thr274
	β I-tubulin	-8.83	2	Pro272, Gln276
	β IIa-tubulin	-8.60	1	Thr274
	β IIb-tubulin	-8.85	2	Thr274, Arg359
	β III-tubulin	-8.46	2	Thr274, Arg359
	β IVa-tubulin	-8.36	2	Thr274, Arg359
	β IVb-tubulin	-8.37	1	Thr274
	β V-tubulin	-8.38	2	Thr274, Arg359
CTX	β VI-tubulin	-8.28	2	Thr274, Arg359
	β VIII-tubulin	-8.78	3	Thr274, Arg359
	β I-tubulin	-8.18	2	Thr274, Gln276
	β IIa-tubulin	-8.69	1	Thr274
	β IIb-tubulin	-8.55	2	His227, Thr274
	β III-tubulin	-8.52	1	His227
	β IVa-tubulin	-8.51	3	His227, Thr274
	β IVb-tubulin	-8.46	3	His227, Thr274, Arg359
	β V-tubulin	-8.24	1	Thr274
	β VI-tubulin	-8.42	2	His227, Thr274
	β VIII-tubulin	-7.92	1	Thr274

According to the docking results, the β I-tubulin and β IIa-tubulin isotypes have stronger binding affinities, and they were selected to perform the following MD simulations.

Molecular dynamics simulations

In order to observe the detailed dynamic process of drug binding, three β -tubulin isotypes (β I-tubulin, β IIa-tubulin, β III-tubulin plus a bound GDP) with three taxanes (PTX, DTX, CTX) were used to construct nine simulation systems. The initial structures were taken from the docking results with the strongest binding affinity, and the MD simulations were carried out for 100 ns. The root mean square deviation (RMSD) analysis suggests that all systems reached their equilibrium structures (Fig. S4 in Supplementary Material), and the deviations in the range of 0.12–0.22 nm indicate that the simulation results are consistent with docking.

For analysis of the complex structures, we evaluated the root mean square of fluctuations (RMSF) for all systems [84]. The RMSF values describe the deviation of an atom in the β -

tubulin (C_{α} atom in the present study) between its instant position and the reference position, which are averaged over the time of simulations. The RMSF values for β I-tubulin, β IIa-tubulin, and β III-tubulin are shown in Fig. S5 (Supplementary Material). The larger RMSF values indicate highly flexible regions, while the smaller RMSF values indicate constrained regions. For the same β -tubulin isotype, the fluctuation patterns are almost the same despite different taxanes, indicating that the action processes for PTX, DTX and CTX are similar.

Most of RMSF peaks are corresponding to the amino acid residues in the random coil structures, which are closed to the ligands and the GDP molecule. As shown in Fig. S5, the amino acid segments 276–284 in all three taxanes (β I-tubulin, β IIa-tubulin, and β III-tubulin) have large RMSF values. However, the RMSF values for the 173–178 amino acid segments in β III-tubulin are higher than those in β IIa-tubulin. For the 37–42 amino acid segments, there are high RMSF values for β I-tubulin, but low values for β III-tubulin. This shows that the ligand has different interactions with the residues on those segments in β III-tubulin.

Figure S6 (Supplementary Material) shows the number of hydrogen bonds between taxanes and tubulin isotypes during the 100 ns simulation processes. For PTX, the most H-bonds are formed between PTX and β Ia-tubulin throughout the process, indicating that PTX has the stronger binding ability to β Ia-tubulin than to the other two β -tubulin isotypes. For DTX, the least H-bonds are formed between DTX and β III-tubulin, indicating weaker binding to β III-tubulin than to β I-tubulin and β Ia-tubulin. However, for CTX, the H-bond numbers between CTX and three β -tubulin isotypes are not so different. In other words, DTX and PTX prefer to bond β Ia-tubulin rather than bond β III-tubulin, while CTX has less selectivity to bond to the three β -tubulin isotypes.

Figure 7 shows the nine equilibrium structures with the key residues after 100 ns of simulation. Figure 7a–c shows the important amino acid residues on β I-tubulin binding with PTX, DTX and CTX. The C13 side chain of DTX and CTX goes deeper into the cavity than PTX of β I-tubulin. This pattern may be related to the big size of the two hydrophobic benzene ring structures on the C13 side chain of PTX. And the main amino acids on β I-tubulin are His227, Glu276, Gln280, and Arg359. Figure 7d–f shows the binding of three

taxanes with β Ia-tubulin. We observed that the orientations of three taxanes are similar, and the important binding amino acids on β Ia-tubulin are His227, Thr274, and Arg276. Figure 7g–i shows the results of three taxanes with β III-tubulin. For different taxanes with β III-tubulin, the orientations of them are different, and the important amino acids on β III-tubulin are also different. Unlike the interaction with β I-tubulin and β Ia-tubulin, the C13 side chain of PTX with β III-tubulin was partially expelled from the cavity, and the overall structure of DTX was expelled. This implies that the interactions of PTX and DTX with β III-tubulin are weak. At the residue level, the interactions of three taxanes with β Ia-tubulin are similar, but with β III-tubulin are quite different.

Based on the MD results, we carried out the MM-PBSA method (with $\epsilon = 2.0$) to study the interactions of the three taxanes on the different β -tubulins (Table 6), while the decomposition of energy terms are listed in Table S5 (Supplementary Material). We also have tried different dielectric constants ($\epsilon = 4.0, 20.0$), and the results are shown in Table S6 (Supplementary Material). Nevertheless, the conclusion for the relative energies is unchanged. According to the literatures [45, 46], the human body mainly consists of the β I-

Fig. 7 The view of the active pockets formed by the key residues (using red sticks) in surface of β -tubulin isotypes binding to taxanes (using rainbow sticks&spheres) after 100 ns of simulation. The important hydrogen bonds are represented by blue dotted lines

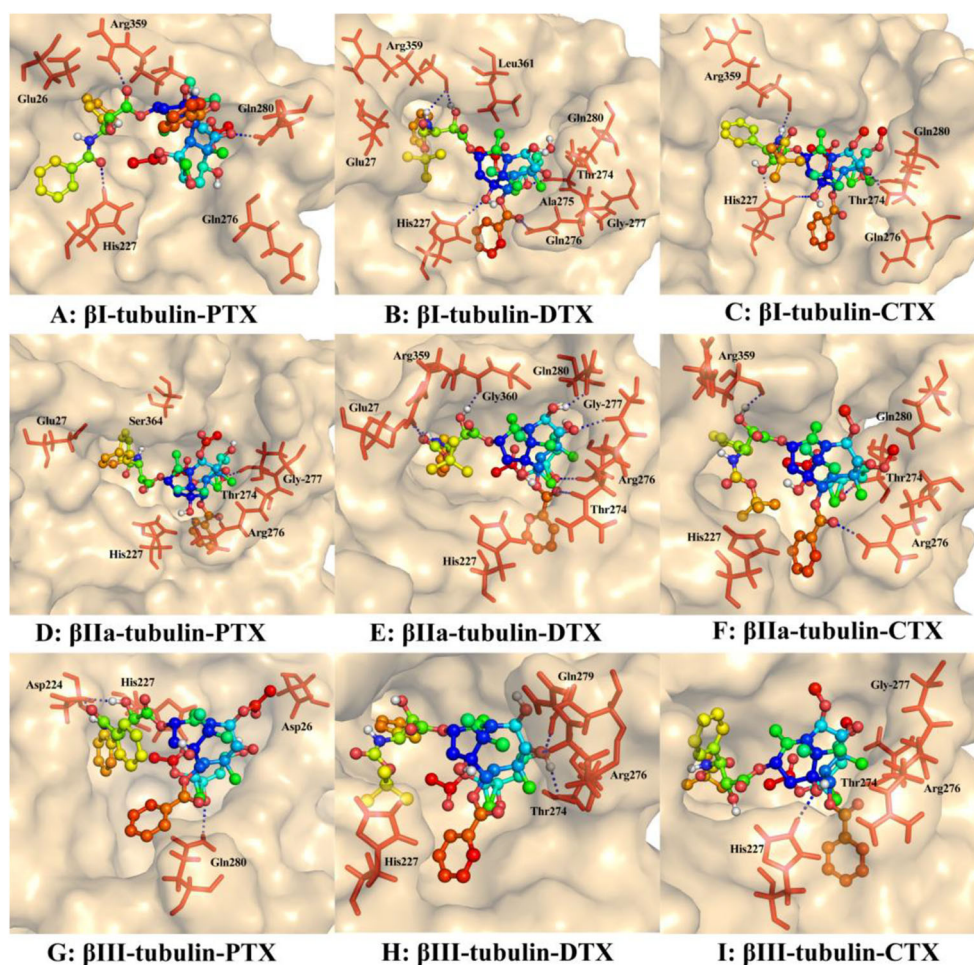


Table 6 The binding free energies of the three taxanes to the three β -tubulin isotypes by MM-PBSA

β -tubulin	Taxane	Binding-free energies (kcal/mol)
β I-tubulin	PTX	-23.1 ± 1.2
	DTX	-29.5 ± 1.6
	CTX	-24.0 ± 2.1
β IIa-tubulin	PTX	-25.5 ± 1.2
	DTX	-29.0 ± 0.5
	CTX	-25.9 ± 1.5
β III-tubulin	PTX	-8.6 ± 1.3
	DTX	-17.8 ± 1.9
	CTX	-23.0 ± 1.4

tubulin and β II-tubulin isotypes in early treatment, and DTX has been used in the clinic as the first-line drugs. As shown in Table 6 and Table S5 (Supplementary Material), the strong binding affinities are predicted between DTX and β I-tubulin (-29.5 kcal/mol) or between DTX and β IIa-tubulin (-29.0 kcal/mol), but weaker interaction between DTX and β III-tubulin (-17.8 kcal/mol). This may be related to the different effects of DTX for different β -tubulins. PTX has a similar situation as DTX. As for CTX, the binding affinity with β III-tubulin (-23.0 kcal/mol) is close to those with β I-tubulin (-24.0 kcal/mol) and with β IIa-tubulin (-25.9 kcal/mol). Interestingly, our theoretical modeling is consistent with the clinical studies. As it was reported, the expression of β III-tubulin in the human body would increase after the treatment with PTX and DTX, and the resistance would occur to PTX and DTX on the later stage [32, 41]. In this case, CTX is used as the second-line drug in the clinic to prolong life, when the patient has resistance to DTX [49].

Conclusions

In this study, the interactions of three taxanes (PTX, DTX, CTX) have been investigated with different human $\alpha\beta$ -tubulin isotypes. Initially, molecular conformations for the drugs were optimized by the DFT methods, and we obtained the low-lying conformations of CTX and their properties, such as their IR spectra and the excited states. Using homology modeling method, we successfully built the 3D models of human $\alpha\beta$ -tubulin isotypes with high identity ($>78\%$) between the template and target proteins. Thus, these models are reliable for the docking and MD simulations. Next, the binding sites of $\alpha\beta$ -tubulin dimer for CTX were found on β -tubulin by molecular docking, and these sites are similar to those for PTX and DTX. The β I-tubulin and β IIa-tubulin isotypes have substantial binding affinities docking with the taxanes.

Finally, we carried out molecular dynamics simulations for β I-tubulin, β IIa-tubulin, and β III-tubulin with the three taxanes. Although the active pockets of different tubulin isotypes with three taxanes are comparable, the key amino acid residues and drug orientations are different. The three taxanes have quite different intermolecular actions on β III-tubulin. The binding affinities of DTX with β I-tubulin and β IIa-tubulin are quite strong, while that on β III-tubulin is relatively weak. On the contrary, the binding affinity of CTX on β III-tubulin is higher than PTX and DTX. Our study supports the use of CTX as the second-line drug for the patients who are resistant to the action of DTX in the clinic. Since our computational outcomes are consistent with the clinical studies of cabazitaxel, these results should be helpful for future experimental studies of taxanes.

Acknowledgments This work was supported by the National Natural Science Foundation of China (grants No. 10904111, 11604238, and 21772146), the Tianjin Natural Science Foundation (11JCYBJC14500), the Science & Technology Development Fund of Tianjin Education Commission for Higher Education (2019KJ175), and the China Postdoctoral Science Foundation (20100470792). We appreciate the supply of the computing resources by USTC. The research at the University of Georgia was supported by the National Science Foundation (Grant CHE-1661604). The visit of MZ to the Center for Computational Quantum Chemistry, the University of Georgia was very helpful.

Compliance with ethical standards

Conflict of interest The authors declare that they have no conflicts of interest.

References

1. Siegel RL, Miller KD, Jemal A (2018) Cancer statistics, 2018. *CA Cancer J. Clin.* 68(1):7–30. <https://doi.org/10.3322/caac.21442>
2. Yan X, Han R, Zhou J, Yu H, Yang J, Wu M (2016) Incidence, mortality and survival of female breast cancer during 2003–2011 in Jiangsu province, China. *Chin J Cancer Res* 28(3):321–329. <https://doi.org/10.21147/j.issn.1000-9604.2016.03.06>
3. Chen W, Zheng R, Baade PD, Zhang S, Zeng H, Bray F, Jemal A, Yu XQ, He J (2016) Cancer statistics in China, 2015. *CA Cancer J. Clin.* 66(2):115–132. <https://doi.org/10.3322/caac.21338>
4. Zeng H, Chen W, Zheng R, Zhang S, Ji JS, Zou X, Xia C, Sun K, Yang Z, Li H, Wang N, Han R, Liu S, Li H, Mu H, He Y, Xu Y, Fu Z, Zhou Y, Jiang J, Yang Y, Chen J, Wei K, Fan D, Wang J, Fu F, Zhao D, Song G, Chen J, Jiang C, Zhou X, Gu X, Jin F, Li Q, Li Y, Wu T, Yan C, Dong J, Hua Z, Baade P, Bray F, Jemal A, Yu XQ, He J (2018) Changing cancer survival in China during 2003–15: a pooled analysis of 17 population-based cancer registries. *Lancet Glob. Health* 6(5):e555–e567. [https://doi.org/10.1016/S2214-109X\(18\)30127-X](https://doi.org/10.1016/S2214-109X(18)30127-X)
5. Chen JG, Chen HZ, Zhu J, Yang YL, Zhang YH, Huang PX, Chen YS, Zhu CY, Yang LP, Shen K, Qiang FL, Wang GR (2018) Cancer survival in patients from a hospital-based cancer registry, China. *J. Cancer* 9(5):851–860. <https://doi.org/10.7150/jca.23039>
6. Janke C, Bulinski JC (2011) Post-translational regulation of the microtubule cytoskeleton: mechanisms and functions. *Nat Rev Mol Cell Biol* 12(12):773–786. <https://doi.org/10.1038/nrm3227>

7. Conde C, Caceres A (2009) Microtubule assembly, organization and dynamics in axons and dendrites. *Nat. Rev. Neurosci.* 10(5): 319–332. <https://doi.org/10.1038/nrn2631>
8. Perez EA (2009) Microtubule inhibitors: differentiating tubulin-inhibiting agents based on mechanisms of action, clinical activity, and resistance. *Mol. Cancer Ther.* 8(8):2086–2095. <https://doi.org/10.1158/1535-7163.MCT-09-0366>
9. Giannakakou P, Gussio R, Nogales E, Downing KH, Zaharevitz D, Bollback B, Poy G, Sackett D, Nicolaou KC, Fojo T (2000) A common pharmacophore for epothilone and taxanes: molecular basis for drug resistance conferred by tubulin mutations in human cancer cells. *Proc. Natl. Acad. Sci.* 97(6):2904–2909. <https://doi.org/10.1073/pnas.040546297>
10. Kruczynski A, Barret JM, Etievant C, Colpaert F, Fahy J, Hill BT (1998) Antimitotic and tubulin-interacting properties of vinflunine, a novel fluorinated vinca alkaloid. *Biochem. Pharmacol.* 55(5): 635–648. [https://doi.org/10.1016/s0006-2952\(97\)00505-4](https://doi.org/10.1016/s0006-2952(97)00505-4)
11. Lu Y, Chen J, Xiao M, Li W, Miller DD (2012) An overview of tubulin inhibitors that interact with the colchicine binding site. *Pharm. Res.* 29(11):2943–2971. <https://doi.org/10.1007/s11095-012-0828-z>
12. Jordan MA, Wilson L (2004) Microtubules as a target for anticancer drugs. *Nat. Rev. Cancer* 4(4):253–265. <https://doi.org/10.1038/nr1317>
13. Ravelli RB, Gigant B, Curmi PA, Jourdain I, Lachkar S, Sobel A, Knossow M (2004) Insight into tubulin regulation from a complex with colchicine and a stathmin-like domain. *Nature* 428(6979): 198–202. <https://doi.org/10.1038/nature02393>
14. Mukhtar E, Adhami VM, Mukhtar H (2014) Targeting microtubules by natural agents for cancer therapy. *Mol. Cancer Ther.* 13(2):275–284. <https://doi.org/10.1158/1535-7163.mct-13-0791>
15. Prota AE, Bargsten K, Zurwerra D, Field JJ, Diaz JF, Altmann KH, Steinmetz MO (2013) Molecular mechanism of action of microtubule-stabilizing anticancer agents. *Science* 339(6119): 587–590. <https://doi.org/10.1126/science.1230582>
16. Field JJ, Diaz JF, Miller JH (2013) The binding sites of microtubule-stabilizing agents. *Chem. Biol.* 20(3):301–315. <https://doi.org/10.1016/j.chembiol.2013.01.014>
17. Blagosklonny MV, Fojo T (1999) Molecular effects of paclitaxel: myths and reality (a critical review). *Int J Cancer* 83(2):151–156. [https://doi.org/10.1002/\(sici\)1097-0215\(19991008\)83:2.3.co;2-5](https://doi.org/10.1002/(sici)1097-0215(19991008)83:2.3.co;2-5)
18. Lowe J, Li H, Downing KH, Nogales E (2001) Refined structure of $\alpha\beta$ -tubulin at 3.5 Å resolution. *J. Mol. Biol.* 313(5):1045–1057. <https://doi.org/10.1006/jmbi.2001.5077>
19. Mitra A, Sept D (2008) Taxol allosterically alters the dynamics of the tubulin dimer and increases the flexibility of microtubules. *Biophys. J.* 95(7):3252–3258. <https://doi.org/10.1529/biophysj.108.133884>
20. Natarajan K, Senapati S (2012) Understanding the basis of drug resistance of the mutants of $\alpha\beta$ -tubulin dimer via molecular dynamics simulations. *PLoS One* 7(8):e42351. <https://doi.org/10.1371/journal.pone.0042351>
21. Alushin GM, Lander GC, Kellogg EH, Zhang R, Baker D, Nogales E (2014) High-resolution microtubule structures reveal the structural transitions in $\alpha\beta$ -tubulin upon GTP hydrolysis. *Cell* 157(5): 1117–1129. <https://doi.org/10.1016/j.cell.2014.03.053>
22. Kellogg EH, Hejab NMA, Howes S, Northcote P, Miller JH, Diaz JF, Downing KH, Nogales E (2017) Insights into the distinct mechanisms of action of taxane and non-taxane microtubule stabilizers from cryo-EM structures. *J. Mol. Biol.* 429(5):633–646. <https://doi.org/10.1016/j.jmb.2017.01.001>
23. Cao YN, Zheng LL, Wang D, Liang XX, Gao F, Zhou XL (2018) Recent advances in microtubule-stabilizing agents. *Eur. J. Med. Chem.* 143:806–828. <https://doi.org/10.1016/j.ejmech.2017.11.062>
24. Sun C, Zhu L, Zhang C, Song C, Wang C, Zhang M, Xie Y, Schaefer HF (2018) Conformers, properties, and docking mechanism of the anticancer drug docetaxel: DFT and molecular dynamics studies. *J. Comput. Chem.* 39(15):889–900. <https://doi.org/10.1002/jcc.25165>
25. Shah M, Dauffenbach L, Kerfoot CA, Cohen P, Culver KW, Sharma S, Wartmann M (2003) A comparative study of two novel, non-taxane microtubule stabilizing agents (XAA296A and EPO906A) utilizing the extreme drug resistance (EDR) assay in paclitaxel-sensitive or paclitaxel-resistant breast and ovarian cancers. *Clin Cancer Res* 9(16):6133s
26. Sgadari C, Toschi E, Palladino C, Barillari G, Carlei D, Cereseto A, Ciccolella C, Yarchoan R, Monini P, Sturzl M, Ensoli B (2000) Mechanism of paclitaxel activity in Kaposi's sarcoma. *J. Immunol.* 165(1):509–517. <https://doi.org/10.4049/jimmunol.165.1.509>
27. Seoud MAF, Shamseddine A, Khalil AM, Charafeddine M, Geara FB (2006) Randomized trial comparing concurrent radiotherapy with cisplatin compared with paclitaxel in cervical cancer. *Obstet Gynecol* 107(4):43S. <https://doi.org/10.1097/00006250-200604001-00101>
28. Von Hoff DD, Goldstein D, Renschler MF (2014) Albumin-bound paclitaxel plus gemcitabine in pancreatic cancer REPLY. *N. Engl. J. Med.* 370(5):479–480
29. McGrogan BT, Gilmartin B, Carney DN, McCann A (2008) Taxanes, microtubules and chemoresistant breast cancer. *Biochim. Biophys. Acta* 1785(2):96–132. <https://doi.org/10.1016/j.bbcan.2007.10.004>
30. Joensuu H, Bono P, Kataja V, Alanko T, Kokko R, Asola R, Utriainen T, Turpeenniemi-Hujanen T, Jyrkkio S, Moykkynen K, Helle L, Ingalsuo S, Pajunen M, Huusko M, Salminen T, Auvinen P, Leinonen H, Leinonen M, Isola J, Kellokumpu-Lehtinen PL (2009) Fluorouracil, epirubicin, and cyclophosphamide with either docetaxel or vinorelbine, with or without trastuzumab, as adjuvant treatments of breast cancer: final results of the FinHer trial. *J. Clin. Oncol.* 27(34):5685–5692. <https://doi.org/10.1200/JCO.2008.21.4577>
31. Gernone A, Pagliarulo A, Calderoni G, Pagliarulo V (2011) Elderly patients with metastatic castrate-resistant prostate cancer (mCRPC): safety and efficacy of docetaxel retreatment. *J Clin Oncol* 29(7): 161. https://doi.org/10.1200/jco.2011.29.7_suppl.161
32. Urano N, Fujiwara Y, Doki Y, Kim SJ, Miyoshi Y, Noguchi S, Miyata H, Takiguchi S, Yasuda T, Yano M, Monden M (2006) Clinical significance of class III β -tubulin expression and its predictive value for resistance to docetaxel-based chemotherapy in gastric cancer. *Int. J. Oncol.* 28(2):375–381
33. Galsky MD, Dritselis A, Kirkpatrick P, Oh WK (2010) Cabazitaxel. *Nat. Rev. Drug Discov.* 9(9):677–678. <https://doi.org/10.1038/nrd3254>
34. Duran GE, Wang YC, Francisco EB, Rose JC, Martinez FJ, Collier J, Brassard D, Vrignaud P, Sikic BI (2015) Mechanisms of resistance to cabazitaxel. *Mol. Cancer Ther.* 14(1):193–201. <https://doi.org/10.1158/1535-7163.MCT-14-0155>
35. Paller CJ, Antonarakis ES (2011) Cabazitaxel: a novel second-line treatment for metastatic castration-resistant prostate cancer. *Drug Des Devel Ther* 5:117–124. <https://doi.org/10.2147/DDDT.S13029>
36. Pean E, Demolis P, Moreau A, Hemmings RJ, O'Connor D, Brown D, Shepard T, Abadie E, Pignatti F (2012) The European Medicines Agency Review of Cabazitaxel (Jevtana®) for the treatment of hormone-refractory metastatic prostate cancer: summary of the Scientific Assessment of the Committee for Medicinal Products for Human Use. *Oncologist* 17(4):543–549. <https://doi.org/10.1634/theoncologist.2011-0364>
37. Luduena RF (1998) Multiple forms of tubulin: different gene products and covalent modifications. *Int. Rev. Cytol.* 178:207–275
38. Santoshi S, Naik PK (2014) Molecular insight of isotypes specific β -tubulin interaction of tubulin heterodimer with noscapinoids. *J.*

- Comput. Aided Mol. Des. 28(7):751–763. <https://doi.org/10.1007/s10822-014-9756-9>
39. Derry WB, Wilson L, Khan IA, Luduena RF, Jordan MA (1997) Taxol differentially modulates the dynamics of microtubules assembled from unfractionated and purified β -tubulin isotypes. *Biochemistry* 36(12):3554–3562. <https://doi.org/10.1021/bi962724m>
 40. Yang CH, Yap EH, Xiao H, Fiser A, Horwitz SB (2016) 2-(m-Azidobenzoyl)taxol binds differentially to distinct β -tubulin isotypes. *Proc. Natl. Acad. Sci.* 113(40):11294–11299. <https://doi.org/10.1073/pnas.1613286113>
 41. Hari M, Yang H, Zeng C, Canizales M, Cabral F (2003) Expression of class III β -tubulin reduces microtubule assembly and confers resistance to paclitaxel. *Cell Motil. Cytoskeleton* 56(1):45–56. <https://doi.org/10.1002/cm.10132>
 42. Seve P, Isaac S, Tredan O, Souquet PJ, Pacheco Y, Perol M, Lafanechere L, Penet A, Peiller EL, Dumontet C (2005) Expression of class III β -tubulin is predictive of patient outcome in patients with non-small cell lung cancer receiving vinorelbine-based chemotherapy. *Clin. Cancer Res.* 11(15):5481–5486. <https://doi.org/10.1158/1078-0432.CCR-05-0285>
 43. Ferrandina G, Martinelli E, Zannoni GF, Distefano M, Paglia A, Ferlini C, Scambia G (2007) Expression of class III β -tubulin in cervical cancer patients administered preoperative radiochemotherapy: correlation with response to treatment and clinical outcome. *Gynecol. Oncol.* 104(2):326–330. <https://doi.org/10.1016/j.ygyno.2006.08.046>
 44. Sève P, Dumontet C (2008) Is class III β -tubulin a predictive factor in patients receiving tubulin-binding agents? *Lancet Oncol* 9(2):168–175. [https://doi.org/10.1016/s1470-2045\(08\)70029-9](https://doi.org/10.1016/s1470-2045(08)70029-9)
 45. Katsetos CD, Herman MM, Mork SJ (2003) Class III β -tubulin in human development and cancer. *Cell Motil. Cytoskeleton* 55(2):77–96. <https://doi.org/10.1002/cm.10116>
 46. Ferrandina G, Zannoni GF, Martinelli E, Paglia A, Gallotta V, Mozzetti S, Scambia G, Ferlini C (2006) Class III β -tubulin overexpression is a marker of poor clinical outcome in advanced ovarian cancer patients. *Clin. Cancer Res.* 12(9):2774–2779. <https://doi.org/10.1158/1078-0432.ccr-05-2715>
 47. Magnani M, Ortuso F, Soro S, Alcaro S, Tramontano A, Botta M (2006) The β I/ β III-tubulin isoforms and their complexes with antimetabolic agents. *FEBS J.* 273(14):3301–3310. <https://doi.org/10.1111/j.1742-4658.2006.05340.x>
 48. Akasaka K, Maesawa C, Shibasaki M, Maeda F, Takahashi K, Akasaka T, Masuda T (2009) Loss of class III β -tubulin induced by histone deacetylation is associated with chemosensitivity to paclitaxel in malignant melanoma cells. *J. Investig. Dermatol.* 129(6):1516–1526. <https://doi.org/10.1038/jid.2008.406>
 49. Smiyun G, Azarenko O, Miller H, Rifkind A, LaPointe NE, Wilson L, Jordan MA (2017) β III-tubulin enhances efficacy of cabazitaxel as compared with docetaxel. *Cancer Chemother. Pharmacol.* 80(1):151–164. <https://doi.org/10.1007/s00280-017-3345-2>
 50. Yusuf RZ, Duan Z, Lamendola DE, Penson RT, Seiden MV (2003) Paclitaxel resistance: molecular mechanisms and pharmacologic manipulation. *Curr. Cancer Drug Targets* 3(1):1–19. <https://doi.org/10.2174/1568009033333754>
 51. Ferlini C, Raspaglio G, Cicchillitti L, Mozzetti S, Prislei S, Bartollino S, Scambia G (2007) Looking at drug resistance mechanisms for microtubule interacting drugs: does TUBB3 work? *Curr. Cancer Drug Targets* 7(8):704–712. <https://doi.org/10.2174/156800907783220453>
 52. Sissung TM, Baum CE, Deeken J, Price DK, Aragon-Ching J, Steinberg SM, Dahut W, Sparreboom A, Figg WD (2008) ABCB1 genetic variation influences the toxicity and clinical outcome of patients with androgen-independent prostate cancer treated with docetaxel. *Clin. Cancer Res.* 14(14):4543–4549. <https://doi.org/10.1158/1078-0432.ccr-07-4230>
 53. Kavallaris M (2010) Microtubules and resistance to tubulin-binding agents. *Nat. Rev. Cancer* 10(3):194–204. <https://doi.org/10.1038/nrc2803>
 54. Kulkarni SA, Feng SS (2011) Effects of surface modification on delivery efficiency of biodegradable nanoparticles across the blood-brain barrier. *Nanomedicine* 6(2):377–394. <https://doi.org/10.2217/nmm.10.131>
 55. Culine S (2018) Refining the use of cabazitaxel in metastatic castrate-resistant prostate cancer. *Eur. J. Cancer* 97:30–32. <https://doi.org/10.1016/j.ejca.2018.04.002>
 56. Zhang ML, Song C, Yao Z, Ji Q (2012) Theoretical studies of the structure and properties of anticancer drug taxol. *Curr Org Chem* 16(19):2321–2331. <https://doi.org/10.2174/138527212803520281>
 57. Durrant JD, McCammon JA (2011) Molecular dynamics simulations and drug discovery. *BMC Biol.* 9:71. <https://doi.org/10.1186/1741-7007-9-71>
 58. Frisch MJ, Trucks GW, Schlegel HB, Scuseria GE, Robb MA, Cheeseman JR, Scalmani G, Barone V, Petersson GA, Nakatsuji H, Li X, Caricato M, Marenich AV, Bloino J, Janesko BG, Gomperts R, Mennucci B, Hratchian HP, Ortiz JV, Izmaylov AF, Sonnenberg JL, Williams, Ding F, Lipparini F, Egidi F, Goings J, Peng B, Petrone A, Henderson T, Ranasinghe D, Zakrzewski VG, Gao J, Rega N, Zheng G, Liang W, Hada M, Ehara M, Toyota K, Fukuda R, Hasegawa J, Ishida M, Nakajima T, Honda Y, Kitao O, Nakai H, Vreven T, Throssell K, Montgomery Jr. JA, Peralta JE, Ogliaro F, Bearpark MJ, Heyd JJ, Brothers EN, Kudin KN, Staroverov VN, Keith TA, Kobayashi R, Normand J, Raghavachari K, Rendell AP, Burant JC, Iyengar SS, Tomasi J, Cossi M, Millam JM, Klene M, Adamo C, Cammi R, Ochterski JW, Martin RL, Morokuma K, Farkas O, Foresman JB, Fox DJ (2016) Gaussian 16 Rev. B.01. Wallingford, CT
 59. Cavasotto CN, Phatak SS (2009) Homology modeling in drug discovery: current trends and applications. *Drug Discov. Today* 14(13–14):676–683. <https://doi.org/10.1016/j.drudis.2009.04.006>
 60. The UniProt C (2017) UniProt: the universal protein knowledgebase. *Nucleic Acids Res.* 45(D1):D158–D169. <https://doi.org/10.1093/nar/gkw1099>
 61. McWilliam H, Li W, Uludag M, Squizzato S, Park YM, Buso N, Cowley AP, Lopez R (2013) Analysis tool web services from the EMBL-EBI. *Nucleic Acids Res.* 41:W597–W600. <https://doi.org/10.1093/nar/gkt376>
 62. Guex N, Peitsch MC, Schwede T (2009) Automated comparative protein structure modeling with SWISS-MODEL and Swiss-PdbViewer: a historical perspective. *Electrophoresis* 30:S162–S173. <https://doi.org/10.1002/elps.200900140>
 63. Benkert P, Biasini M, Schwede T (2011) Toward the estimation of the absolute quality of individual protein structure models. *Bioinformatics (Oxford, England)* 27(3):343–350. <https://doi.org/10.1093/bioinformatics/btq662>
 64. Bienert S, Waterhouse A, de Beer TA, Tauriello G, Studer G, Bordoli L, Schwede T (2017) The SWISS-MODEL repository—new features and functionality. *Nucleic Acids Res.* 45(D1):D313–D319. <https://doi.org/10.1093/nar/gkw1132>
 65. Bertoni M, Kiefer F, Biasini M, Bordoli L, Schwede T (2017) Modeling protein quaternary structure of homo- and hetero-oligomers beyond binary interactions by homology. *Sci. Rep.* 7(1):10480. <https://doi.org/10.1038/s41598-017-09654-8>
 66. Waterhouse A, Bertoni M, Bienert S, Studer G, Tauriello G, Gumienny R, Heer FT, de Beer TAP, Rempfer C, Bordoli L, Lepore R, Schwede T (2018) SWISS-MODEL: homology modeling of protein structures and complexes. *Nucleic Acids Res.* 46(W1):W296–W303. <https://doi.org/10.1093/nar/gky427>
 67. Gilson MK, Zhou HX (2007) Calculation of protein-ligand binding affinities. *Annu. Rev. Biophys.* 36:21–42. <https://doi.org/10.1146/annurev.biophys.36.040306.132550>

68. Morris GM, Huey R, Lindstrom W, Sanner MF, Belew RK, Goodsell DS, Olson AJ (2009) AutoDock4 and AutoDockTools4: automated docking with selective receptor flexibility. *J. Comput. Chem.* 30(16):2785–2791. <https://doi.org/10.1002/jcc.21256>
69. Van Der Spoel D, Lindahl E, Hess B, Groenhof G, Mark AE, Berendsen HJ (2005) GROMACS: fast, flexible, and free. *J. Comput. Chem.* 26(16):1701–1718. <https://doi.org/10.1002/jcc.20291>
70. Wang J, Wolf RM, Caldwell JW, Kollman PA, Case DA (2004) Development and testing of a general amber force field. *J. Comput. Chem.* 25(9):1157–1174. <https://doi.org/10.1002/jcc.20035>
71. Leontyev IV, Stuchebrukhov AA (2010) Electronic polarizability and the effective pair potentials of water. *J. Chem. Theory Comput.* 6(10):3153–3161. <https://doi.org/10.1021/ct1002048>
72. Hess B (2008) P-LINCS: a parallel linear constraint solver for molecular simulation. *J. Chem. Theory Comput.* 4(1):116–122. <https://doi.org/10.1021/ct700200b>
73. Mozzetti S, Ferlini C, Concolino P, Filippetti F, Raspaglio G, Prislei S, Gallo D, Martinelli E, Ranelletti FO, Ferrandina G, Scambia G (2005) Class III β -tubulin overexpression is a prominent mechanism of paclitaxel resistance in ovarian cancer patients. *Clin. Cancer Res.* 11(1):298–305
74. Seve P, Mackey J, Isaac S, Tredan O, Souquet PJ, Perol M, Lai R, Voloch A, Dumontet C (2005) Class III β -tubulin expression in tumor cells predicts response and outcome in patients with non-small cell lung cancer receiving paclitaxel. *Mol. Cancer Ther.* 4(12):2001–2007. <https://doi.org/10.1158/1535-7163.MCT-05-0244>
75. Gan PP, Pasquier E, Kavallaris M (2007) Class III β -tubulin mediates sensitivity to chemotherapeutic drugs in non-small cell lung cancer. *Cancer Res.* 67(19):9356–9363. <https://doi.org/10.1158/0008-5472.CAN-07-0509>
76. Guo J, Wang X, Sun H, Liu H, Yao X (2012) The molecular basis of IGF-II/IGF2R recognition: a combined molecular dynamics simulation, free-energy calculation and computational alanine scanning study. *J. Mol. Model.* 18(4):1421–1430. <https://doi.org/10.1007/s00894-011-1159-4>
77. Jing X, Xiaoqiang H, Yushan Z (2019) Using molecular dynamics simulations to evaluate active designs of cephradine hydrolase by molecular mechanics/Poisson – Boltzmann surface area and molecular mechanics/generalized born surface area methods. *RSC Adv.* 9:13868–13877. <https://doi.org/10.1039/c9ra02406a>
78. Kumari R, Kumar R, Open Source Drug Discovery C, Lynn A (2014) g_mmpbsa—a GROMACS tool for high-throughput MM-PBSA calculations. *J. Chem. Inf. Model.* 54(7):1951–1962. <https://doi.org/10.1021/ci500020m>
79. Stepanian SG, Reva ID, Radchenko ED, Adamowicz L (1998) Conformational behavior of α -alanine. Matrix-isolation infrared and theoretical DFT and ab initio study. *J Phys Chem A* 102(24):4623–4629. <https://doi.org/10.1021/jp973479z>
80. Yu D, Kang W, Hao F, Li Z (2017) Spectroscopic studies and structural elucidation of cabazitaxel. *Chinese J Magn Reson* 34(2):191–199
81. Baker D, Sali A (2001) Protein structure prediction and structural genomics. *Science* 294(5540):93–96. <https://doi.org/10.1126/science.1065659>
82. Bowie JU, Luthy R, Eisenberg D (1991) A method to identify protein sequences that fold into a known three-dimensional structure. *Science* 253(5016):164–170
83. Luthy R, Bowie JU, Eisenberg D (1992) Assessment of protein models with three-dimensional profiles. *Nature* 356(6364):83–85. <https://doi.org/10.1038/356083a0>
84. Kumbhar BV, Borogaon A, Panda D, Kunwar A (2016) Exploring the origin of differential binding affinities of human tubulin isotypes $\alpha\beta$ II, $\alpha\beta$ III and $\alpha\beta$ IV for DAMA-colchicine using homology modelling, molecular docking and molecular dynamics simulations. *PLoS One* 11(5):e0156048. <https://doi.org/10.1371/journal.pone.0156048>

Publisher's note Springer Nature remains neutral with regard to jurisdictional claims in published maps and institutional affiliations.